The Cryosphere Discuss., 9, 1269–1313, 2015
www.the-cryosphere-discuss.net/9/1269/2015/
doi:10.5194/tcd-9-1269-2015

The Cryosphere Discussions
Open Access

Satellite passive microwave measurements of sea ice concentration: an optimal algorithm and challenges

N. Ivanova[1], L. T. Pedersen[2], R. T. Tonboe[2], S. Kern[3], G. Heygster[4], T. Lavergne[5], A. Sørensen[5], R. Saldo[6], G. Dybkjær[2], L. Brucker[7,8], and M. Shokr[9]

[1]Nansen Environmental and Remote Sensing Center, Bergen, Norway
[2]Danish Meteorological Institute, Copenhagen, Denmark
[3]University of Hamburg, Hamburg, Germany
[4]University of Bremen, Bremen, Germany
[5]Met-Norway, Oslo, Norway
[6]Technical University of Denmark, Lyngby, Denmark
[7]NASA Goddard Space Flight Center, Cryospheric Sciences Laboratory, Code 615, Greenbelt, Maryland 20771, USA
[8]Universities Space Research Association, Goddard Earth Sciences Technology and Research Studies and Investigations, Columbia, Maryland 21044, USA
[9]Environment Canada, Ontario, Canada

Received: 4 February 2015 – Accepted: 14 February 2015 – Published: 26 February 2015

Correspondence to: N. Ivanova (natalia.ivanova@nersc.no)

Published by Copernicus Publications on behalf of the European Geosciences Union.

Abstract

Sea ice concentration has been measured globally with satellite microwave radiometers for over 30 years. However there is still a need for better understanding of corresponding challenges and consequently identifying an optimal method for sea ice concentration retrieval suitable for climate monitoring. The method should minimize inter-sensor calibration discrepancies and sensitivity to error sources with climatic trends (e.g. atmospheric water vapour and water surface roughening by wind). This article presents the results of an extensive algorithm inter-comparison and validation experiment. Thirty sea ice algorithms entered the experiment where their skills were evaluated over low and high sea ice concentrations, thin ice and areas covered by melt ponds. In addition, atmospheric correction of input brightness temperatures and dynamic tie-points approach were suggested. A selection of thirteen algorithms is shown in the article to demonstrate the results. Based on the findings, an optimal approach was suggested to retrieve sea ice concentration globally for climate monitoring purposes.

1 Introduction

From a climate change perspective, it is important to know how fast the total volume of sea ice is changing. In addition to sea ice thickness, this requires reliable estimates of sea ice concentration (SIC). Consistency in sea ice climate records is, in turn, crucial for understanding of internal variability and external forcing in the observed sea ice retreat in the Arctic (Notz and Marotzke, 2012) and expansion in the Antarctic (Parkinson and Cavalieri, 2012).

Precision and accuracy serve as measures of performance of a SIC algorithm. Precision (represented by the SD) is the range within which repeated retrievals of the same quantity scatter around the true value. Accuracy (represented by the bias) is the difference between the mean retrieval and the true value. Average accuracy of com-

TCD
9, 1269–1313, 2015

monly known algorithms, such as NASA Team (Cavalieri et al., 1984) and Bootstrap (Comiso, 1986), is reported to be within ±5 % in winter in a compact (high concentration) ice pack. A comparison of seven algorithms to a trusted dataset of Synthetic Aperture Radar (SAR) and ship-based observations in the Arctic showed the precision of 3–5 %, including sensor noise (Andersen et al., 2007). In summer and at the ice edge the uncertainty can be more than ±20 % (Meier and Notz, 2010). These uncertainties are in general caused by atmospheric contributions, wind roughening of open water areas, variations in sea ice emissivity, sensor noise (Andersen et al., 2006, 2007). Inter-comparison of eleven sea ice algorithms in the Arctic showed differences in SIC retrievals among the algorithms of 2.0–2.5 % in winter in the areas of consolidated ice (5–12 % for intermediate SIC) and 2–8 % in summer reaching up to 12 % in the Canadian Archipelago area (Ivanova et al., 2014).

There are two main error sources, to which the algorithms have different response. The first is the sensitivity to emissivity and physical temperature of sea ice. This depends on the selection of input brightness temperatures used to calculate SIC as well as on internal properties of the algorithms. Input brightness temperatures are available at electromagnetic frequencies between 6 and near 90 GHz in vertical (V) and horizontal (H) polarisations. Kwok (2002) and Andersen et al. (2007) showed that SIC algorithms do not reflect the near 100 % ice concentration variability in the Arctic adequately; variability due to actual ice concentration changes in the order of less than 3 % is below the noise floor of the algorithms. Heat and moisture fluxes between the surface (ocean or ice) and atmosphere are sensitive to small variations in the near 100 % ice cover. These discrepancies can thus be of significant importance for sea ice models (and consequently coupled climate models) when assimilating these data without proper handling of the uncertainties. The apparent fluctuations in the derived ice concentration in the near 100 % ice regime are primarily attributed to snow/ice surface emissivity variability around the tie-point signature and only secondarily to actual ice concentration fluctuations (Kwok, 2002).

TCD
9, 1269–1313, 2015

The second error source is the effect of atmospheric constituents such as water vapour and cloud liquid water. It causes the observed brightness temperature to change as a function of polarisation and frequency, as well as season and location. This effect is usually larger during summer and early fall and over open water (also in the marginal ice zone) because of the larger amounts of water vapour and cloud liquid water in the atmosphere. In addition to atmospheric extinction, wind roughening of the water surface causes the surface emissivity to change towards the values typical for sea ice (Andersen et al., 2006).

Algorithms with different sensitivities to surface emission and atmospheric effects produce different estimates of trends in sea ice area and extent on seasonal and decadal time scales (Andersen et al., 2007). This means that not only does the sea ice area have a climatic trend, but also trends in atmospheric and surface constituents affecting the microwave emission may impose additional effects. Trends in wind patterns, atmospheric water vapour and liquid water content (Wentz et al., 2007), snow depth and snow properties, and the fraction of perennial ice could have such effects.

However, some algorithms are less sensitive than others to these effects, and it is important to select an algorithm with low sensitivity. It is particularly important to have low sensitivity to error sources for which it is at the present time impossible to correct, e.g. extinction and emission by cloud liquid water or ice particles, or sea ice emissivity variability. We therefore designed a set of experiments to test a number of aspects related to sea ice algorithm performance, ultimately to allow us to select an optimal algorithm for retrieval of a SIC climate data record.

Melt ponds on Arctic summer sea ice represent an additional source of errors due to their microwave radiometric signatures being similar to open water. Virtually all SIC algorithms based on the passive microwave channels around 19, 37, and 90 GHz are very sensitive to presence of melt water on the ice. The depth of penetration of microwave radiation into liquid water is a few millimetres at most, and therefore it is impossible to distinguish between ocean water (in leads) and melt water (on the ice). This is the primary reason why most SIC algorithms are less reliable during summer

TCD
9, 1269–1313, 2015

and potentially underestimate the actual SIC (Fetterer and Untersteiner, 1998; Cavalieri et al., 1990; Comiso and Kwok, 1996). Melt ponds may exhibit a diurnal cycle with interchanging periods of open water and thin ice. This further complicates the SIC retrieval using satellite microwave radiometry during summer and increases the level of uncertainty. Sea ice algorithms are known to underestimate SIC by up to 40 % in the areas with melt ponds (Rösel et al., 2012b).

Thin ice is known to be another challenge for the passive microwave algorithms as they underestimate SIC in such areas (Heygster et al., 2014). Aerial (Naoki et al., 2008) and satellite (Heygster et al., 2014) passive microwave measurements show an increase in brightness temperature with sea ice thickness (< 30 cm), which is more pronounced for lower frequencies and horizontal polarisation. Since an instantaneous amount of thin ice can reach as much as 1 million km^2 (total amount globally, Grenfell et al., 1992), the effect of SIC underestimation can be significant for ice volume estimates, air–sea heat exchange and modelled ice dynamics. It is suggested that the dependency of brightness temperature on the sea ice thickness is due to changes in near-surface dielectric properties caused, in turn, by changes of brine salinity with thickness and temperature (Naoki et al., 2008).

For the first time this many (thirty) algorithms have been assessed in a consistent manner including both hemispheres, and their performance tested with regard to high and low SIC, areas with melt ponds, thin ice, atmospheric influence and tie-points; and covering the properties of the Scanning Multichannel Microwave Radiometer (SMMR), Special Sensor Microwave/Imager (SSM/I) and Advanced Microwave Scanning Radiometer for the Earth Observing System (AMSR-E). When evaluating the algorithms we have in particular focused on achieving low sensitivity to the error sources over ice and open water, performance in areas covered by melt ponds in summer and thin ice in autumn. We suggest that an optimal algorithm should be adaptable to: (1) dynamic tie-points in order to reduce inter-instrument biases and sensitivity to climatological trends in error sources and (2) regional error reduction using meteorological data and forward models.

TCD
9, 1269–1313, 2015

The algorithms evaluation was carried out in the context of European Space Agency Sea Ice Climate Change Initiative (ESA SICCI) and is described in the following sections. Section 2 describes the algorithms and the basis for selection of the thirteen algorithms to be shown in the following sections. Section 3 describes the data and methods. Section 4 presents the main results of the work: algorithms validation and evaluation, suggested atmospheric correction and dynamic tie-points approach. The discussion and conclusions are provided in Sects. 5 and 6, respectively.

2 The algorithms

During the experiment we have implemented 30 SIC algorithms and found that they form groups according to their main principle. We also found that algorithms within each group have very similar sensitivities to atmospheric effects and surface emissivity variations, which is in agreement with sensitivity studies (Tonboe, 2010; Tonboe et al., 2011) using simulated brightness temperatures generated by coupling a thermodynamic ice/snow model to the Microwave Emissivity Model for Layered Snow Packs. To avoid redundancy we only include here a selection of 13 sea ice algorithms (Table 1), which were chosen as representatives of the groups.

2.1 Selected algorithms

The first group of algorithms, represented by Bootstrap polarisation mode (BP), includes the polarisation algorithms. These algorithms primarily use 19 or 37 GHz polarisation difference (difference between brightness temperatures in vertical and horizontal polarisations of the same frequency) or polarisation ratio (polarisation difference divided by the sum of the two brightness temperatures). The next group uses 19 and 37V channels and is represented here by CalVal (CV). Commonly known algorithms in this group are NORSEX (Svendsen et al., 1983), Bootstrap Frequency Mode (BF, Comiso, 1986) and UMass-AES (Swift et al., 1985). Bristol (BR) represents the group that uses

TCD
9, 1269–1313, 2015

both polarisation and spectral gradient information by deploying channels: 19, 37V and 37H. The NASA Team algorithm (NT) uses the polarisation ratio at 19 GHz and gradient ratio at 19 and 37V. ASI (a non-linear algorithm) and Near 90 GHz linear (N90) use the polarisation difference at near 90 GHz. These are also called near 90 GHz or high-frequency algorithms. ESMR (named after the single channel 18H radiometer on board Nimbus-5 operating from 1972 to 1977) and 6H are one-channel algorithms using horizontal polarisation of 18/19 and 6 GHz channels respectively. ECICE and NASA Team 2 (NT2) represent a special class of more complex algorithms where more channels are used and where additional data may be needed as input. Finally we consider combinations of algorithms (hybrid algorithms), where one of the algorithms is expected to have low sensitivity to atmospheric effects over open water, and the other is expected to have a better performance over ice. This group includes the NT+CV: an average of NT and CV, the CV+N90: an average of N90 and CV, and the OSISAF: a weighted combination of BR over ice and BF over open water (note that BF is identical to CV).

2.2 Tie-points

A necessary parameter for practically every algorithm is a set of tie-points. Tie-points are typical radiometric measurements of sea ice (100 % SIC) and open water (0 % SIC) used to assign each pixel with a given observed radiometric parameter to ice or open water. Under certain conditions such as wind-roughened water surface or thin sea ice it is difficult to define a single tie-point to represent the surface. In nature, brightness temperature may have a range of variability from same ice type or open water due to varying emissivity, atmospheric conditions, and temperature of the emitting layer. Therefore the retrieved sea ice concentrations scatter near the tie-points that correspond to 0 and 100 % may lead to negative or larger than 100 % concentrations. ECICE uses the probability distribution of the radiometric observation from each surface, instead of a single tie-point, to represent the surface.

In order to obtain an unbiased comparison of the algorithms, we have developed a special set of tie-points (Table A1) based on our reference round robin data pack-

TCD
9, 1269–1313, 2015

age (RRDP) for both hemispheres and for each of the three radiometers: AMSR-E, SSM/I and SMMR. This enables us to compare the algorithms directly without biases between the algorithms caused by a different choice of tie-points. These tie-points are used for all the algorithms except NASA Team 2 and ECICE where such traditional tie-points are not applicable and the original implementations of these algorithms were used. We refer to the text leading to Eqs. (1) and (2) further down to understand how we could include these two algorithms into our inter-comparison nevertheless. All the algorithms were evaluated without applying open water/weather filter, since our aim was a comparison of the algorithms themselves. We consider performance of an open water/weather filter separately in Sect. 4.4.

3 The data and validation/evaluation procedure

3.1 The input data

Single swath brightness temperatures were used as input to the algorithms. The SMMR data were obtained from the US National Snow and Ice Data Centre – NSIDC (25 October 1978 to 20 August 1987; Njoku, 2003), EUMETSAT CM-SAF provided the SSM/I data (covering 9 July 1987 to 31 December 2008; Fennig et al., 2013), and AMSR-E data were from NSIDC (from 19 June 2002 to 3 October 2011; Ashcroft and Wentz, 2003).

It is important to note that different datasets may have different calibration, and it can even be the case for different versions of the same dataset. Therefore the results presented in the following (especially the derived tie-points) should only be applied to other datasets with some caution.

3.2 The validation data

Ideally, every algorithm should be evaluated over open water, at intermediate concentrations and at near 100 % ice cover. In practise, it is difficult to find high quality ref-

TCD
9, 1269–1313, 2015

erence data at intermediate concentrations especially for large areas covering entire satellite footprint (e.g. 70 km × 45 km for SSM/I at 19.3 GHz) and covering all seasons and ice types. Since the relationship between SIC and brightness temperatures at all frequencies is assumed linear (except for the various noise contributions and a slight nonlinearity of the ASI algorithm), we argue that performance at intermediate concentrations can be found as linear combination of performances at 0 and 100 %. Thus a Round Robin Data Package (RRDP) was built for validation of the algorithms at 0 and 100 % SIC.

For the Open Water (OW) validation dataset (SIC = 0 %), areas of open water were found using ice charts from Danish Meteorological Institute (DMI) and the US National Ice Center (NIC). The validation dataset for 0 % SIC covered the following time periods: 1978–1987 (SMMR), 1987–2008 (SSM/I), and 2002–2011 (AMSR-E). For this paper we used the subsets of 1978–1985 for SMMR, 1988–2008 for SSM/I and the full AMSR-E dataset.

To create the Closed Ice (CI) validation dataset (SIC = 100 %), areas of convergence were identified in ENVISAT ASAR derived sea ice drift fields (available from the PolarView and MyOcean projects). The basic assumption for the convergence method to provide 100 % sea ice is that during winter after 24 h of net convergence the open water areas (leads) have either closed or got refrozen. During summer, this assumption does not hold due to the presence of melt-ponds and the lack of refreezing. The CI dataset is therefore only valid for accurate tests during winter (October–April in the Northern Hemisphere and May–September in the Southern Hemisphere). The CI dataset covered years 2007–2008 for SSM/I and 2007–2011 for AMSR-E. SMMR was not included, because there were no SAR data available at the time of SMMR.

Figure 1 (Northern Hemisphere) and Fig. 2 (Southern Hemisphere) show the coverage of a subset of the RRDP for the SSM/I instrument during winter seasons of 2007 and 2008. The coverage of the RRDP is displayed both in terms of Brightness Temperatures (Tb) in the 6 channels of the SSM/I instrument (main panels), and in terms of spatial distribution (embedded maps). In all panels, square symbols are used for

TCD
9, 1269–1313, 2015

the OW dataset, and circles are used for the CI dataset. In the Tb diagrams, the OW symbols are coloured according to Tb22V values (left colour scale), while the CI symbols are coloured according to Tb37H values (right colour scale). The colouring of CI symbols is also used in the embedded maps.

The left hand side panels of Figs. 1 and 2 show the RRDP SSM/I subset in a classic (Tb37V, Tb19V) space, which is the one sustaining the BF algorithm (or CV). The ice line extends along different ice types. In the Northern Hemisphere, ice types vary from multi-year sea ice (MYI) with lower values of Tb37H (colouring) to first year ice (FYI) with higher values of Tb37H. In the Southern Hemisphere, the ice line extends between ice types A, representing FYI, and B, sea ice with a heavy snow cover (Gloersen et al., 1992). The so-called FYI and MYI tie-points would typically lie along this line. The location of these different ice types can be seen on the embedded maps, and matches the expected distribution of older and younger ice in the Northern Hemisphere. In the (Tb37V, Tb19V) space, the OW samples are grouped mostly in one point (OW tie-point), but also present some spread due to the geophysical noise induced by atmosphere (water vapour, liquid water- and ice clouds) and surface variability (wind, temperature). The Tb22V colouring of the OW symbols illustrates how the variability of the OW signature is mostly driven by factors impacting also the 22 GHz channel (atmospheric water vapour content). The length and orientation of the OW spread, and especially the distance from the OW points to the line of ice points, determines the strength of algorithms built on these frequencies (e.g. BF or CV) at low ice concentrations.

The right hand side panel shows the same data but in a (Tb85V, Tb85H) space. The ice line is very well defined (limited lateral spread), almost with a slope of unit. On the other hand, it is difficult to define an OW point in this axis, since samples are now spread along a line. This "weather line" even intersects the ice line, illustrating that algorithms based purely in the (Tb85V, Tb85H) space (like the ASI and N90 algorithms) will have difficulty at discriminating open water from sea ice under certain atmospheric conditions.

TCD
9, 1269–1313, 2015

The embedded maps display the winter location of the OW samples (same location for the whole RRDP, for all instruments). In both hemispheres, these locations follow sea ice retreat in summer months to always capture ocean/atmosphere conditions in the vicinity of sea ice (not shown). The observed hole near the North Pole is due to the ENVISAT ASAR not covering north of 87°. The somewhat limited coverage of the sea ice samples of the Pacific sector in the Northern Hemisphere and many areas in the Southern Hemisphere is due to scene acquisition strategies of the ENVISAT SAR mission.

Some algorithms have a special way of estimating tie-points and a non-linear way of dealing with ice concentrations near 0 and 100 % or they use simple truncation at 0 and 100 %. This complicates comparison of these algorithms directly to other algorithms because the SD of the retrieved ice concentration is affected by the treatment at the 0 and 100 % reference points. Therefore, we have produced reference datasets of brightness temperatures in every channel that correspond to values of SIC 15 and 75 % for an additional evaluation. A bias at these intermediate reference points will indicate a bias at intermediate concentrations in general.

The 15 % dataset was constructed by mixing the average FYI signature (brightness temperature) with the OW dataset i.e.

$$\mathrm{Tb15} = 0.85 \cdot \mathrm{Tb}(t) + 0.15 \cdot \mathrm{Tb100}\left(\overline{\mathrm{FY}}\right), \quad (1)$$

where Tb0 (OW brightness temperature) is multiplied by 0.85 (85 % water) and is varying with time, while the added 15 % FYI signature is an average value constant for all data points from the RRDP (see above) for a given year. By using the 15 % dataset we aim at testing sensitivity of the algorithms to atmospheres over the ocean and not to variability in emissivity of ice. Therefore we keep Tb of ice constant.

The 75 % dataset was generated similarly to the 15 % dataset, but with full variability of ice and 25 % of the average OW signature:

$$\mathrm{Tb75} = 0.75 \cdot \mathrm{Tb100}(t) + 0.25 \cdot \mathrm{Tb0}\left(\overline{\mathrm{OW}}\right). \quad (2)$$

TCD
9, 1269–1313, 2015

For the 75 % SIC dataset the variability in brightness temperatures is driven by variability at SIC 100 %, and not at SIC 0 %. We keep SIC 0 % brightness temperature constant in order to avoid mixing the atmospheres, which would have happened if we mixed variable SIC 100 % brightness temperatures with variable SIC 0 % brightness temperatures. As a consequence, the SIC 75 % dataset will reflect a lower atmospheric variability than we would have to expect from a real SIC 75 % dataset. Since the CI dataset is only valid for the winter season, the same applies for this 75 % dataset.

The 15 and 75 % reference datasets are constructed to be able to compare algorithms and their SD at intermediate concentrations and to compare algorithms with nonlinearities near 100 % ice concentration (e.g. ASI) and algorithms with large positive biases when implemented without open water filter (e.g. ASI and NASA Team 2). It is noteworthy that we originally had designed a 85 % reference dataset, but the positive biases of these two algorithms were larger than 15 % and thus part of the SD was still cut-off at 100 %. Therefore it was necessary to use a 75 % dataset instead. The performance of the algorithms was consistent between the 75, 85 and 100 % datasets, and therefore we consider such substitute acceptable. This way of mixing brightness temperatures is not entirely physical since we are mixing brightness temperatures seen through two different atmospheres. However, since the majority of the signal originates from either open water or ice, and we use fixed brightness temperatures for the remaining fraction, we consider the results to be still reasonably representative for algorithm performance evaluation.

Normally, SIC products are truncated at 0 and 100 % to allow only physically meaningful SIC values. Although, this does not apply to ECICE because it employs the inequality constraint of 0 % < SIC < 100 % in its optimization formulation. However, as the intention here is to investigate the statistical properties of the retrievals, we will analyse actual SIC as retrieved with the algorithms, without truncation, which means the retrieved values can be negative or above 100 %. Instrument and geophysical noise cause the brightness temperatures to vary around the chosen tie-points, and it cannot

TCD
9, 1269–1313, 2015

be avoided that at least a part of this noise is translated into some noise in the SIC retrieved.

3.3 Reference data for melt-pond sensitivity assessment

Daily gridded SIC and melt pond fraction reference dataset for the Arctic (Rösel et al., 2012a) was derived from clear-sky measurements of reflectances in channels 1, 3 and 4 of the MODerate resolution Imaging Spectroradiometer (MODIS) of June, July, and August 2009. The melt pond fraction is determined using a classification based on a mixed-pixel approach. It is assumed that the reflectance measured over each MODIS 500 m × 500 m grid cell comprises contributions from three surface types: melt ponds, open water, sea ice/snow (Rösel et al., 2012a). By using known reflectance values (e.g. Tschudi et al., 2008) a neural network was built, trained, and applied (Rösel et al., 2012a). Melt pond fractions are given as the fraction of the sea ice that has melt ponds. For the mentioned time period 16 520 grid cells (100 km × 100 km each) contained melt ponds under clear-sky (< 10 % cloud cover) and above 90 % MODIS SIC. For the sensitivity analysis a total of 8152 data points were selected from this dataset, so that SD of melt pond fraction over each 100 km × 100 km area was less than 5 %, SIC variations were less than 5 %, and SIC itself was larger than 95 %.

3.4 Reference data for the thin ice tests

Sensitivity of the algorithms to thickness of thin (≤ 50 cm) sea ice was evaluated. For this purpose a thin ice thickness dataset was compiled by manually identifying large (100 km diameter) areas of ∼ 100 % homogenous thin ice areas in the Arctic Ocean using ENVISAT ASAR WSM (Advanced Synthetic Aperture Radar, Wide Swath Mode) data (175 scenes), and subsequently deriving thin ice thickness for these areas using ESA's L-band Soil Moisture and Ocean Salinity (SMOS) sensor (Huntemann et al., 2014; Heygster et al., 2014). The dataset covers the time period from 1 October to 12 December 2010 and consists of 991 measurements of sea ice thickness. For these

TCD
9, 1269–1313, 2015

selected grid cells AMSR-E brightness temperatures were extracted and used as input to the SIC algorithms.

3.5 Atmospheric correction and weather filters

SIC retrievals can be contaminated due to wind roughening of the ocean surface, atmospheric water vapour and cloud liquid water, and precipitation. Traditionally, the atmospheric effects on the SIC retrievals are dealt with by applying an open water/weather filter based on gradient ratios of brightness temperatures (Tb), see Gloersen and Cavalieri (1986) for SMMR and Cavalieri et al. (1995) for SSM/I:

$$\text{SMMR}: \quad \text{SIC} = 0 \quad \text{if } GR(18/37) > 0.07 \tag{3}$$

$$\text{SSM/I}: \quad \text{SIC} = 0 \quad \text{if } GR(19/37) > 0.05 \quad \text{and/or } GR(19/22) > 0.045, \tag{4}$$

where the gradient ratios of Tb18V (Tb19V) and Tb37V (GR(18/37) and GR(19/37)) are most sensitive to cloud liquid water and the gradient ratio of Tb19V and Tb22V (GR(19/22)) mainly detects water vapour. We test the performance of this technique in Sect. 4.4. Following Andersen et al. (2006) and Kern (2004) we suggest an alternative to the open water/weather filter. The suggested method consists of applying a more direct atmospheric correction methodology, where the input brightness temperatures from SSM/I (in all the channels used by the algorithms) are corrected with regard to atmospheric and surface effects using a Radiative Transfer Model (RTM) (Wentz, 1997). Fields of 10 m wind speed, total columnar water vapour, and air temperature at 2 m from the ECMWF ERA-Interim Numerical Weather Prediction (NWP) re-analysis are used in this process (3 hourly maps). Following the results of Andersen et al. (2006) we did not use cloud liquid water and precipitation from the NWP data because these are considered to be less consistent with the observed brightness temperatures (reconfirmed by our own analysis). The NWP model grid points are collocated with the AMSR-E/SSM/I swath brightness temperatures in time and space. Using the 3 hourly NWP fields we ensure a time difference between the NWP data and the satellite data to be within 1.5 h.

TCD
9, 1269–1313, 2015

3.6 The validation/evaluation procedure

Brightness temperatures from the three microwave radiometer instruments (AMSR-E, SSM/I and SMMR) were extracted and collocated with the reference datasets introduced above for open water, closed ice, melt ponds, and thin ice in a so-called Round Robin Data Package (RRDP). These TB data were then used as input to the algorithms to retrieve SIC. It is noted that the RRDP, including all the reference data, collocated brightness temperatures and SIC retrievals, is available upon request to anyone interested in inter-comparing, improving or developing SIC algorithms (http://esa-seaice-cci.org).

The criteria for the validation and evaluation procedure were based on the desire to minimize the sensitivities to atmosphere attenuation and surface emissivity as described in the Introduction. In addition, we considered following aspects: (1) data record length: algorithms using near 90 GHz channels cannot be used before 1991 when the first functional SSM/I 85 GHz radiometer started to provide consistent data, (2) spatial resolution: ranges from over 100 km to less than 10 km for different channels and instruments, (3) performance along the ice edge, where new ice formation is common in winter, and (4) performance during the summer melt. Additional criteria for the algorithm selection were: the possibility of reducing regional error using, e.g. NWP data and forward models; and the possibility to use dynamic tie-points to reduce sensitivity to inter-sensor calibration differences and global and regional climatological trends in error sources (Andersen et al., 2006)

4 Results

4.1 Sea ice algorithms inter-comparison and validation

To assess performance of the algorithms, bias and SD from the validation dataset were calculated for the Northern (Fig. 3, upper panels) and the Southern (Fig. 3, bottom pan-

TCD
9, 1269–1313, 2015

els) Hemispheres for the instruments AMSR-E, SSM/I and SMMR (shown in different symbols in the figures) during summer (empty symbols) and winter (filled symbols). The algorithms are sorted by the average (of all the cases) values of the bias (left hand side, the average is calculated from absolute values) and the SD, which is shown by the grey bars (right hand side). The averages of SDs are weighted by the number of years when data were available for each instrument, thus giving more weight to SSM/I as the one providing the longest dataset. Only cases of 15 and 75 % are shown because they reflect the performance of the algorithms for low and high concentrations respectively and can be used to test all algorithms. Thus, 0 and 100 % are not shown (except SMMR, for which 0 % is shown as a replacement for 15 %) but they produced very similar results for the algorithms that could be tested with these (see Sect. 3). There are no data for high concentrations in summer for the reasons explained in Sect. 3 (presence of melt ponds and lack of refreezing).

Here we divide the algorithms in low-frequency, high-frequency and very-low-frequency (6H) algorithms due to each instruments temporal coverage. AMSR-E (9.5 years, July 2002–2011) provides data for all the groups. SSM/I data were available for the low-frequency algorithms during 20 years (1988–2008) and for high-frequency algorithms during 16 years (1992–2008). The SSM/I instruments did not include 6 GHz channels, therefore the very low frequency (6H) algorithm does not apply to the SSM/I data. SMMR did not have high frequencies and thus only applies to low- and very-low-frequency algorithms (7.2 years, November 1978–1987).

The high-frequency algorithms ASI and N90 have a clear difference between the low and high concentration performance (SDs), the same is true for the CV+N90 algorithm, but the separation is smaller as this hybrid algorithm also contains a low-frequency component (Fig. 3., right). The large SDs for these algorithms mainly originate from the low concentration cases, where the atmospheric influence is more pronounced than for low-frequency algorithms. Winter SDs for most of the algorithms tend to be lower than the ones of summer (the filled symbols are usually below the empty ones in the same category of concentration and instrument).

TCD
9, 1269–1313, 2015

In the Northern Hemisphere the stronger negative biases tend to be caused by the high concentration cases (with the exception of the N90, CV+N90, NT2 and ASI), while stronger positive biases are caused by the low concentration cases. Algorithms ASI, NT2 and ECICE are positively biased for all the cases in both hemispheres. Note that the ECICE algorithm was adjusted for the Northern Hemisphere in this study. These three algorithms are the only ones for which it was not possible to use the RRDP tie-points as was done for the other algorithms, and this may explain part of the bias (see Sect. 4.5 for further discussion on tie-points). For the algorithms with large biases, the bias influences (reduces) our ability to estimate their SD properly using the chosen approach and thus makes them look better than they really are at intermediate (high) concentrations. It is noted that in the Fig. 3 some of the summer biases for SIC 15 % in the Southern Hemisphere are hidden behind the winter values (BR, NT+CV, CV, ESMR, ECICE and NT2).

Difference in SD between summer and winter in both hemispheres is lowest for the CV algorithm, having also the 4th smallest average SD in the Northern Hemisphere and the 2nd smallest average SD in the Southern Hemisphere. The other algorithms with relatively low summer-winter difference in SD are NT+CV, NT, OSISAF and Bristol. On average for all the five algorithms the difference amounts to 0.1–0.3 % for AMSR and SSM/I at SIC = 15 %, and higher for the other algorithms (0.4–1.2 %).

4.2 Melt ponds

The SIC and melt pond fraction estimates from MODIS were collocated with coincident daily SIC retrieved by the passive microwave algorithms in the Arctic Ocean for June to August 2009 to investigate the sensitivity of the algorithms to melt ponds.

From the MODIS melt pond fraction (MPF, the fraction of ice that is covered by melt ponds) and MODIS SIC (MSIC) data the net area fraction of ice (C) is calculated as

$$C = (1 - W) = \mathrm{MSIC} - \mathrm{MSIC} \cdot \mathrm{MPF}, \quad (5)$$

TCD
9, 1269–1313, 2015

where W is surface fraction of water (leads + melt ponds). We compute this net ice area fraction because we expect that passive microwave SIC algorithms interpret melt ponds as open water and hence yield a SIC which is 1 minus the fraction of leads minus the fraction of melt ponds. Figure 4 shows SIC calculated by four selected sea ice algorithms (CV, BR, N90 and NT) as a function of C. Note that because of the limitation to MSIC > 95 % the variation in the net ice area fraction is almost solely due to the variation in MPF, which was varying from 0 to 50 % for the selected dataset.

There is a pronounced overestimation of the net ice area fraction by the CalVal and Bristol algorithms that compose the OSISAF combination (however only Bristol is used for high SIC). For example, at $C = 90$ % the average SIC is 128 % (CalVal), 115 % (Bristol), 103 % (Near90) and 100 % (NASA Team). The SIC values obtained by the four algorithms are correlated to C (correlation coefficients: 0.57 for NT, 0.84 for CV and BR, and 0.60 for N90). This agrees with the assumption that melt ponds are interpreted as open water by microwave radiometry, because C represents pure ice (the melt pond fraction and leads are excluded). The algorithms N90 and NT seem to have less sensitivity to the melt ponds, which may be caused by them being less affected by surface temperature variations as they are based on polarisation difference (N90) and polarisation and gradient ratios (NT). The NASA Team algorithm shows the SIC values closest to C (the least bias of the four algorithms), which adds to our argument for using this algorithm for defining areas of high SIC (NT > 95 %) for retrieval of the dynamic tie-points (Sect. 4.5).

4.3 Thin ice

Sensitivity of selected sea ice algorithms (CV, BR, OSISAF, N90, NT and 6H) to thin sea ice thickness is investigated. Figure 5 shows SIC obtained by the algorithms as a function of sea ice thickness from SMOS (see Sect. 3 for details). The data are shown as averages for each sea ice thickness bin of 5 cm width with the number of measurement in each bin shown on the figure (total number of measurements 991). The grey shading shows SD, which is calculated from all the SIC retrievals in the given

TCD
9, 1269–1313, 2015

bin. The SDs are calculated for each algorithm, but overlap each other on the figure. Since in the OSISAF combination the Bristol has weight of 1 for high concentrations, these algorithms show identical results; therefore Bristol is not visible.

The SIC is known to be ~ 100 % for the cases selected, therefore one would expect all the curves to be near horizontal and placed at high SIC. However, this is not going to be the case following published knowledge suggesting that SIC is underestimated for thin ice (e.g. Grenfell et al., 1992). Hence, we are interested in the point where a given algorithm is no longer affected by the ice thickness. All the algorithms underestimate the SIC for ice thickness up to 25 cm. Note that most of the algorithms also show a negative bias of about 5 % for ice thickness above 30 cm, i.e. ice which is not termed thin ice anymore. This could be caused by the fact that the thin ice identified in SAR images is on average smoother/less deformed and most likely has less snow than the ice used for the derivation of the sea ice tie-points applied in the algorithms.

Out of the five algorithms shown, Near90 levels off, that is the SIC value varies by less than 5 % between the neighbouring bins of SIT, at the lowest thicknesses (20–25 cm). The OSISAF and CalVal follow at the thicknesses of 25–30 cm, and NASA Team and 6H at 30–35 cm. The slightly better performance of CV relative to OSISAF suggests a shift in the mixing of BR and CV in a new algorithm (using CV at higher intermediate concentrations), see the introduction of the SICCI algorithm in the discussion section.

More details on the algorithm's performance over thin ice can be found in Heygster et al. (2014).

4.4 Atmospheric correction

We implement the traditional open water/weather filters according to Eqs. (1) and (4), which work as ice-water classifiers. They set pixels, classified as subjected to a high atmospheric influence over open water, to 0 % ice concentration. This efficiently removes noise due to the weather influence in open water regions.

However, we find, as did also Andersen et al. (2006), that open water/weather filter also eliminates real low concentration ice (up to 30 %). This is illustrated in Fig. 6, where

TCD
9, 1269–1313, 2015

intermediate concentration datasets were generated using equations similar to Eq. (1) from the same brightness temperatures as used for the algorithms inter-comparison (Sect. 4.1). The filter identifies correctly the pixels, which do not contain any ice (SIC = 0 %): practically all pixels are located outside the red square in the upper left plot. The filter keeps almost all the pixels containing sea ice (SIC = 30 %): almost all pixels are located inside the red square in the bottom right plot; only a handful values falls outside the range defined by the red box and is set to 0 %. However for the cases of SIC 15 and 20 %, which are shown here as an example, the filter sets SIC to 0 % for all the pixels outside the red square in the upper right and bottom left plots, which corresponds to 27 % of the total amount of pixels (3320) for the SIC 15 % and to 9 % for the SIC 20 %.

In order to avoid this truncation of real SIC by the open water/weather filter, we investigate an alternative approach where we apply atmospheric correction to the brightness temperatures, as described in Sect. 3, before using them as input to the algorithms. The correction reduced the brightness temperature variance by 22–35 % (for 19VH and 37VH channels) and up to 40 % (for near 90VH channels) when water vapour, wind speed and 2 m-temperature were used in the correction scheme. Adding cloud liquid water (CLW) as the fourth parameter worsened the results (19VH and 37VH channels). CLW has high spatial and temporal variability and the current ERA Interim resolution and performance for CLW is not sufficient for this correction. In the following the satellite data are therefore not corrected for the influence of CLW.

To illustrate the effect of the correction of the Tbs for the atmospheric influence, we compare the SD of SIC computed from Tbs with and without correction for columnar water vapour, wind speed and 2 m-temperature (Fig. 7). The top plots show histograms of the SIC over open water for the OSISAF algorithm before the correction (left) and after (right). The distribution becomes clearly less noisy and tends to be more Gaussian-shaped. To show the effect of the correction on performance of all the algorithms (except NT2 and ECICE), the SD is shown in the bottom plot. The SD has decreased by 48–65 % after the atmospheric correction for all the shown algorithms. It should be

TCD
9, 1269–1313, 2015

noted that the tie-points need to be adjusted to the atmospherically corrected data. The tie-points given in Table A1 are for uncorrected data.

4.5 Dynamic tie-points

As mentioned in the Introduction, not only sea ice extent has a trend, but also atmospheric and surface effects influencing the microwave emission measured at the satellite could have a trend. In order to compensate for these effects, we suggest that in an optimal approach tie-points should be derived dynamically. We suggest using a two-week running window (±7 days) to reduce potential noise in daily values. In order to generate the 100 % ice tie-point we used areas with ice concentrations larger than 95 % from the NASA Team algorithm. The ice tie-point was subsequently calculated as the average brightness temperature value of these selected data points. The NASA Team algorithm was chosen for this purpose because it is a standard relatively simple algorithm with little sensitivity to ice temperature variations (Cavalieri et al., 1984). Only samples at a distance of 100 km from the coast regions, and inside monthly climatology of ice were used. The procedure yielded in the order of 15 000 data points in a two-week period. The data for the open water tie-point were selected geographically along two belts in the Northern and Southern Hemispheres defined by the monthly maximum climatological ice extent (200 km wide belt starting 150 km away from the climatology). Data points south of 50N in the Northern Hemisphere were not used. Total number of data points was limited to 5000 (selected randomly between available points).

Figure 8 shows examples of dynamic tie-points for overlapping periods of the DMSP SSM/I platforms: f10, f11, f13, f14 and f15. The dynamic tie-point for ice is represented by an average of the fraction of FYI and MYI in the samples of all (±7 days) selected ice conditions (NT > 95 %). Due to the change in the relative amount of FYI and MYI in the Arctic Ocean in recent years, the ice average tie-point will move along the ice-line in the brightness temperature space. An example of ice tie-point is presented in Fig. 8a and c by y component of the tie-point space of Bristol algorithm, the algorithm used for high SIC in the OSISAF combination. In the Bristol algorithm the polarization and frequency

TCD
9, 1269–1313, 2015

information from 19, 37V and 37H channels is transformed into a 2-D plane defined by x and y components. The y component shown here as an example is defined as $y = 0.9164\mathrm{Tb19V} - \mathrm{Tb37V} + 0.4965\mathrm{Tb37H}$ (see Smith, 1996 for more details) and is approximately proportional to SIC. The open water tie-points at Tb19V and Tb37V (Fig. 8b and d) are taken from the CalVal/Bootstrap F scheme, the algorithm used at low SIC by the OSISAF.

Figure 8 demonstrates that the tie-points are not constant values as it is assumed traditionally (static tie-points), but rather geophysical parameters showing seasonal and inter-annual variations. Therefore the dynamic approach is more suitable for the SIC algorithms. The left panels in Fig. 8 show that the ice tie-point may vary by about 8 K during one year in the Northern Hemisphere and by about 10 K in the Southern Hemisphere. These values amount to approximately 8–10 % of the average value. Note that even though unit K is applicable to the y-component in the Bristol space it does not represent a brightness temperature in a single channel (see the definition of y above). The seasonal variability for the open water tie-point is smaller (within 5 K).

Another important aspect is a sensor drift and inter-sensor differences, which might cause undesirable trend in the retrieved SIC when static tie-points are applied. The dynamic tie-point approach compensates for these effects. A table of the trend values for the tie-points from Fig. 8 is included as Table B1. All the trends are computed over the same period relative to the season (always from 7 May in the first year considered to 6 May in the last year considered). The trends between different platforms tend to agree within 0.1 $\mathrm{K\,yr^{-1}}$ for both hemispheres (see the values for different platforms in the same overlap period rows). The only exception is for f10 and f11 in the Southern Hemisphere with 0.14 $\mathrm{K\,yr^{-1}}$ difference between the trend values. Inter-sensor biases can be observed as offsets between the different coloured curves in Fig. 8 (see Table B1 with an example of average values for BR ice tie point).

TCD
9, 1269–1313, 2015

5 Discussion

5.1 Algorithms inter-comparison and selection

Based on validation datasets of SIC 15 and 75 % we use variability (SD) in the SIC produced by the different algorithms as a measure of the sensitivity to geophysical error sources and instrumental noise. The errors from geophysical sources over open water are generated by wind induced surface roughness, surface and atmospheric temperature variability and water vapour and cloud liquid water in the atmosphere. Over ice, the errors are dominated by snow and ice emissivity and temperature variability, where parameters such as snow depth, and to some extent variability in snow density and ice emissivity are important (Tonboe and Andersen, 2004). The atmosphere plays only a minor role over ice except at near 90 GHz where liquid water/ice clouds may still be a severe error source, especially in the Marginal Ice Zone. At the same time near 90 GHz data might be less sensitive to changes in physical properties in ice and snow because of the smaller penetration depth compared to the other frequencies used.

The algorithms 6H, OSISAF, CalVal, Bristol and NT+CV showed the lowest SDs in both hemispheres (Fig. 3). The 6 GHz channel was not available on SSM/I, which provides the longest time series, and therefore 6H is not considered to be an optimal algorithm for climate dataset. Bristol has shown the lowest SD over high concentrations (only winter is considered) while CV had the lowest SD for the low concentration cases, which suggests that combining these two algorithms would provide a good basis for an optimal algorithm.

The differences in SDs between summer and winter are reflecting the sensitivity of different algorithms to wind, atmospheric humidity and other seasonally changing quantities. Some of the quantities, such as melt season length or atmospheric opacity, may have climatological trends and therefore small difference between the summer and winter SDs is an asset for an algorithm. The algorithms NT+CV, NASA Team, CalVal, OSISAF and Bristol showed the lowest summer-winter differences in SD (0.1–0.3 % on average for AMSR and SSM/I, 15 % SIC). Note that CV and BF (not shown in the

TCD
9, 1269–1313, 2015

results section) follow the same principle and use the same brightness temperatures and hence perform identically.

5.2 The SICCI algorithm

During the algorithm validation and inter-comparison exercise the SICCI algorithm was introduced. It is a slightly modified version of the OSISAF algorithm in order to achieve better performance for thin ice. Similarly to the OSISAF algorithm, it is constructed as a weighted combination of the CV and BR algorithms. In order to take more advantage of the better performance of CV for thin ice, the weights are defined as follows. For SIC below 70 %, as obtained by CV, the weight of this algorithm is $w_{CV} = 1$, while for high values (≥ 90 %) it is $w_{CV} = 0$. For the intermediate values the weight for CV is defined as

$$w_{CV} = 1 - \frac{SIC_{CV} - 0.7}{0.2}, \quad (6)$$

where SIC_{CV} is SIC (between 0 and 1) obtained by CV. The weight of BR is $1 - w_{CV}$.

In the original OSISAF algorithm, values of 0 and 40 % were used instead of 70 and 90 % suggested here.

5.3 Melt ponds

Figure 4 illustrates that the four algorithms shown (as well as all other algorithms) are sensitive to the melt pond fraction, which may mean that melt ponds are interpreted as open water by the algorithms. This is because microwave penetration into water is very small. Rösel et al. (2012a) showed that in melt-pond infested areas passive microwave algorithms (ASI, NT2 and Bootstrap) underestimate SIC by up to 40 % (corresponding to a MPF of 40 %). However, the algorithms shown in Fig. 4 overestimate SIC. The overestimation can be caused by higher brightness temperature values in the areas between melt ponds. During summer these areas comprise wet snow and/or bare ice with

TCD
9, 1269–1313, 2015

a different physical structure than during winter at temperatures around 0 °C. Therefore these areas have radiometric properties which potentially differ a lot from those present during winter for which the RRDP ice tie-points were developed. The comparison of passive microwave algorithms and MODIS SIC in Rösel et al. (2012b) shows that in the areas without melt ponds the passive microwave SIC is larger than that of MODIS. Note also that the tie-points used here differ from those in Rösel et al. (2012b). Using the dynamic tie-points approach (Sect. 4.5) decreases this effect: OSISAF algorithm on average overestimated SIC by 24 % when fixed RRDP tie-points were used (same as on the Fig. 4) and by 17 % with dynamical tie-points (this example is not shown in the figure). However, even with dynamic tie-points (Sect. 4.5), it is likely that the areas selected to derive the 100 % ice tie-point during summer contain melt ponds. If this would be the case and if the selected area would have an average melt-pond fraction of 10 %, then the 100 % ice tie-point would not represent 100 % ice but a net ice area fraction of only 90 %. When estimating dynamic tie-points, an initial estimate of the ice concentration is needed. In our case this was done using pixels with NT SIC > 95 %. This estimate should be provided by a method, which is sensitive to melt ponds, in order to avoid introducing a bias to the tie-points with melt-pond infested measurements.

5.4 Thin ice

All the algorithms shown for the thin ice test (Fig. 5) underestimate the SIC for ice thicknesses up to 35 cm, which confirms findings by others (see Sect. 1). The 6H algorithm showed the highest sensitivity to the sea ice thickness, which is in agreement with Scott et al. (2014) showing that it is suitable to measure thin ice thickness. The least sensitivity to thickness of thin ice was observed for the N90 algorithm, the SIC obtained by this algorithm was independent of SIT values already at 20–25 cm thicknesses. It is most likely caused by a smaller penetration depth in the near 90 GHz channels (shorter wave length). OSISAF and CalVal had the second least sensitivity (levelled off at 25–30 cm), which adds more weight to the choice of an OSISAF-like combination as an optimal algorithm. Implementation of an algorithm that accounts for thin ice (Röhrs and

TCD
9, 1269–1313, 2015

Kaleschke, 2012; Naoki et al., 2008; Grenfell et al., 1992) as an additional module to this optimal algorithm can be a potential improvement of this drawback.

5.5 Atmospheric correction

Using the emission and radiative transfer model (RTM) of Wentz (1997), we concluded that over open water, most of the algorithms are sensitive to cloud liquid water although the sensitivities of CV and 6H are small (not shown). We found that the representation of cloud liquid water in the NWP data were not suitable for correction of brightness temperatures, which makes it important to select a less sensitive algorithm (e.g. CV). The Bootstrap P, ASI and Near 90 were very sensitive to this component (not shown). Most of the algorithms are sensitive to water vapour over open water especially the BP, ASI and N90. Some of the algorithms show some sensitivity to wind (ocean surface roughness) e.g. NT and BR. But the water vapour and wind roughening we corrected for by applying the RTM correction (see Fig. 7).

It was found that atmospheric correction of brightness temperatures for wind speed, water vapour and temperature reduces the SD in retrieved SIC for all tested algorithms at low concentrations. In addition, the shape of SIC distribution gets closer to Gaussian after the correction (Fig. 7). The OSISAF combination (19V/37V) improved significantly after correction over open water. A simple correction using surface temperature at 100 % was not effective, as considered algorithms showed similar SDs after it was applied (not shown). The atmospheric influence over ice is small and the correction may to some extent introduce noise from the NWP data.

5.6 Dynamic tie-points

The set of static tie-points developed during the RRDP for the algorithm intercomparison differs from the original tie-points (provided with the algorithms). This is caused by the fact that we use different versions of the satellite data, which may have different calibrations. Also, the tie-points published with the algorithms are typically valid

TCD
9, 1269–1313, 2015

for one instrument and need to be derived for each new sensor. The dynamic tie-point method in principle compensates for inter-sensor differences in a consistent manner, so no additional attempt was considered necessary to compensate explicitly for sensor drift or inter-sensor calibration differences (the SSM/I data have been inter-calibrated but not with the SMMR dataset).

We argue that if a geophysical parameter causes a trend in the parameters shown in Fig. 8, this trend should be practically the same across all DMSP platforms. However, the trend would not agree if it were caused by a combination of sensor drift and trend in geophysical parameter. The trends seem to agree according to Table B1 (see Sect. 4.5). It could still be considered as good practice to combine data from different platforms not only for better data coverage but also for mitigating across-platform biases.

The seasonal cycle in the tie-points can be tracked across platforms (Fig. 8). Thus, the tie-points are naturally changing geophysical parameters (or quantities obtained from such parameters), and should be dynamic as opposed to the traditional static approach.

6 Conclusions

A SIC algorithm for climate time series should have low sensitivity to error sources, especially those that we cannot correct for and those which may have climatic trends. When correcting for errors it is important to adjust the tie-points in order to avoid introducing artificial trends from the auxiliary data sources (e.g. NWP data). Therefore the preferred algorithm should have relatively low sensitivity to the tie-points and it should be possible to adjust the tie-points dynamically. The latter is necessary to compensate for climatic changes in the radiometric signature of ice and water; and eventual instrument drift and inter-instrument biases. In addition, this algorithm should be accurate over the whole range of ice concentrations from 0 to 100 %. Along the ice edge spatial resolution and sensitivity to new ice and atmospheric effects is of particular concern.

TCD
9, 1269–1313, 2015

In order to produce a long climate data record, it is also important that the algorithm is based on a selection of channels for which the processing of long time-series is possible, which are currently 19 and 37 GHz. The comprehensive algorithm inter-comparison study reported here leads to following conclusions:

- the CalVal algorithm is among the best (low SD and bias, Fig. 3) of the simple algorithms at low concentrations and over open water;
- the Bristol algorithm is the best (lowest SD and bias, Fig. 3) for high concentrations;
- OSISAF-like combination of CalVal and Bristol is a good choice for an overall algorithm, using CalVal at low concentrations and Bristol at high concentrations.

In addition we conclude that:

- melt ponds are interpreted as water by all algorithms;
- thin ice is seen as reduced concentration by all algorithms;
- after atmospheric correction of brightness temperatures, low concentrations become less uncertain (less noisy) than high concentrations;
- near 90 GHz algorithms are very sensitive to atmospheric effects at low SIC;
- all the 10 algorithms tested improve substantially when brightness temperatures are corrected for atmospheric influence using RTM with NWP data. The additional 3 algorithms by nature could not be corrected/tested for this;
- the dynamic tie-points approach can reduce systematic biases in ice concentration and alleviate the seasonal variability in ice concentration accuracy.

It is clear from these conclusions that not one single algorithm is superior in all criteria and it seems that a combination of algorithms such as the OSISAF/SICCI algorithm is

TCD
9, 1269–1313, 2015

a good choice. An additional advantage of using a set of 19 and 37 GHz algorithms is that the dataset extends from fall 1978 until today and into the foreseeable future.

Over ice the chosen Bristol algorithm is sensitive to the snow and ice temperature profile as well as to ice emissivity variations. Among the ice parameters the surface temperature is the only one, which is quantified in most NWP models. This means that there is a potential for correction. The Bristol performance over melting ice is good because the SIC as a function of net ice fraction has a slope close to 1. The Bristol algorithm as other algorithms has a clear seasonal cycle in the apparent ice concentration at 100 % SIC when using static tie-points. This means that dynamic tie-points are an advantage when using Bristol (as with most other algorithms).

Over open water the CalVal algorithm is among the algorithms with the lowest overall sensitivity to error sources including surface temperature, wind, and atmospheric water vapour. In particular the CalVal is relatively insensitive to cloud liquid water, which is a parameter we cannot correct for due to the uncertainty of this parameter in the NWP data at high latitudes. The response of CalVal to atmospheric correction gives a substantial reduction in the noise level. The response of CalVal to new ice is better than other 19 and 37 GHz algorithms and comparable to near 90 GHz algorithms.

Therefore we recommend an OSISAF/SICCI type of algorithm with dynamic tie-points and atmospheric correction to be used for climate dataset retrievals. The selection of tie-points should be done with careful attention to melt pond issues in order to avoid melt pond contamination of the tie-points in summer. Correction for wind speed, water vapour and surface temperature produces a clear noise reduction, but we found no improvement from correcting for NWP cloud liquid water.

In spite of their high resolution and good skill over ice, the near 90 GHz algorithms have some drawbacks for climatological time series because the near 90 GHz data are not available until 1991 and they are very sensitive to the error sources over open water and near the ice edge such as cloud liquid water. Their skill over ice is approximately the same as the selected Bristol algorithm.

TCD
9, 1269–1313, 2015

Acknowledgements. This work is completed in scope of ESA Sea Ice Climate Change Initiative (SICCI) and was funded by ESA. The work of S. Kern was supported by the Center of Excellence for Climate System Analysis and Prediction (CliSAP). Support from the International Space Science Institute (ISSI), Bern, Switzerland, under project No. 245: Heil P. and S. Kern, "Towards an integrated retrieval of Antarctic sea ice volume".

References

Andersen, S., Tonboe, R., Kern, S., and Schyberg, H.: Improved retrieval of sea ice total concentration from spaceborne passive microwave observations using numerical weather prediction model fields: an intercomparison of nine algorithms, Remote Sens. Environ., 104, 374–392, 2006.

Andersen, S., Tonboe, R., Kaleschke, L., Heygster, G., and Pedersen, L. T.: Intercomparison of passive microwave sea ice concentration retrievals over the high-concentration Arctic sea ice, J. Geophys. Res., 112, C08004, doi:10.1029/2006JC003543, 2007.

Ashcroft, P. and Wentz, F. J.: AMSR-E/Aqua L2A Global Swath Spatially-Resampled Brightness Temperatures, Version 2, NASA DAAC at the National Snow and Ice Data Center, Boulder, Colorado USA, doi:10.5067/AMSR-E/AE_L2A.002, 2003.

Cavalieri, D. J., Gloersen, P., and Campbell, W. J.: Determination of sea ice parameters with the NIMBUS 7 SMMR, J. Geophys. Res., 89, 5355–5369, 1984.

Cavalieri, D. J., Burns, B. A., and Onstott, R. G.: Investigation of the effects of summer melt on the calculation of sea ice concentration using active and passive microwave data, J. Geophys. Res., 95, 5359–5369, 1990.

Cavalieri, D. J., Germain, K. S., and Swift, C. T.: Reduction of weather effects in the calculation of sea ice concentration with the DMSP SSM/I, J. Glaciol., 41, 455–464, 1995.

Comiso, J. C.: Characteristics of arctic winter sea ice from satellite multispectral microwave observations, J. Geophys. Res., 91, 975–994, 1986.

Comiso, J. C. and Kwok, R.: Surface and radiative characteristics of the summer Arctic sea ice cover from multisensor satellite observations, J. Geophys. Res., 101, 28397–28416, 1996.

Eastwood, S. (Ed.): Ocean & Sea Ice SAF (OSISAF) Sea Ice Product Manual, Version 3.8., available at: http://osisaf.met.no, last access: May 2012

TCD
9, 1269–1313, 2015

Fennig, K., Andersson, A., and Schröder, M.: Fundamental Climate Data Record of SSM/I Brightness Temperatures, Satellite Application Facility on Climate Monitoring, doi:10.5676/EUM_SAF_CM/FCDR_SSMI/V001, 2013.
Fetterer, F. and Untersteiner, N.: Observations of melt ponds on Arctic sea ice, J. Geophys. Res., 103, 24821–24835, 1998.
Gloersen, P. and Cavalieri, D. J.: Reduction of weather effects in the calculation of sea ice concentration from microwave radiances, J. Geophys. Res., 91, 3913–3919, 1986.
Gloersen, P., Campbell, W. J., Cavalieri, D. J., Comiso, J. C., Parkinson, C. L., and Zwally, H. J.: Arctic and Antarctic Sea Ice, 1978–1987: satellite passive microwave observations and analysis, NASA SP-511, NASA, Washington, D.C., 1992.
Grenfell, T. C., Cavalieri, D. J., Comiso, J. C., Drinkwater, M. R., Onstott, R. G., Rubinstein, I., Steffen, K., and Winebrenner, D. P.: Considerations for microwave remote sensing of thin sea ice, in: Microwave Remote Sensing of Sea Ice, edited by: Carsey, F. D., American Geophysical Union, Washington, D.C., doi:10.1029/GM068p0291, 1992.
Heygster, G., Huntemann, M., Ivanova, N., Saldo, R., and Pedersen, L. T.: Response of passive microwave sea ice concentration algorithms to thin ice, Proceedings Geoscience and Remote Sensing Symposium (IGARSS), 2014 IEEE International, 13–18 July, Quebec City, QC, 3618–3621, doi:10.1109/IGARSS.2014.6947266, 2014.
Huntemann, M., Heygster, G., Kaleschke, L., Krumpen, T., Mäkynen, M., and Drusch, M.: Empirical sea ice thickness retrieval during the freeze-up period from SMOS high incident angle observations, The Cryosphere, 8, 439–451, doi:10.5194/tc-8-439-2014, 2014.
Ivanova, N., Johannessen, O. M., Pedersen, L. T., and Tonboe, R. T.: Retrieval of Arctic sea ice parameters by satellite passive microwave sensors: a comparison of eleven sea ice algorithms, IEEE T. Geosci. Remote, 52, 7233–7246, 2014.
Kaleschke, L., Lupkes, C., Vihma, T., Haarpaintner, J., Bochert, A., Hartmann, J., and Heygster, G.: SSM/I Sea ice remote sensing for mesoscale ocean–atmosphere interaction analysis, Can. J. Remote Sens., 27, 5, 526–537, 2001.
Kern, S.: A new method for medium-resolution sea ice analysis using weather-influence corrected Special Sensor Microwave/Imager 85 GHz data, Int. J. Remote Sens., 25, 4555–4582, 2004.
Kwok, R.: Sea ice concentration estimates from satellite passive microwave radiometry and openings from SAR ice motion, Geophys. Res. Lett., 29, 1311, doi:10.1029/2002GL014787, 2002.

TCD
9, 1269–1313, 2015

Mäkynen, M., Kern, S., Rösel, A., and Pedersen, L. T.: On the estimation of melt pond fraction on the Arctic Sea ice with ENVISAT WSM images, IEEE T. Geosci. Remote, 52, 7366–7379, 2014.

Markus, T. and Cavalieri, D. J.: An enhancement of the NASA Team sea ice algorithm, IEEE T. Geosci. Remote, 38, 1387–1398, 2000.

Meier, W. and Notz, D.: A note on the accuracy and reliability of satellite-derived passive microwave estimates of sea-ice extent, Clic Arctic sea ice working group, Consensus document, CLIC International Project Office, Tromsø, Norway, 28 October 2010.

Naoki, K., Ukita, J., Nishio, F., Nakayama, M., Comiso, J. C., and Gasiewski, A: Thin sea ice thickness as inferred from passive microwave and in situ observations, J. Geophys. Res., 113, 2156–2202, 2008.

Njoku, E. G.: Nimbus-7 SMMR Pathfinder Brightness Temperatures, 25 October 1978–20 August 1987, NASA DAAC at the National Snow and Ice Data Center, NASA, Boulder, Colorado, USA, 2003.

Notz, D. and Marotzke, J.: Observations reveal external driver for Arctic sea-ice retreat, Geophys. Res. Lett., 39, L08502, doi:10.1029/2012GL051094, 2012.

Parkinson, C. L. and Cavalieri, D. J.: Antarctic sea ice variability and trends, 1979–2010, The Cryosphere, 6, 871–880, doi:10.5194/tc-6-871-2012, 2012.

Parkinson, C. L., Comiso, J. C., and Zwally, H. J.: Nimbus-5 ESMR Polar Gridded Sea Ice Concentrations, 1978–2011, edited by: Meier, W. and Stroeve, J., NASA DAAC at the National Snow and Ice Data Center, NASA, Boulder, Colorado, USA, 2004.

Pedersen, L. T.: Merging microwave radiometer data and meteorological data for improved sea ice concentrations, EARSeL Adv. Remote Sens., 3, 81–89, 1994.

Ramseier, R. O.: Sea ice validation, in: DMSP Special Sensor Microwave/Imager Calibration/Validation, edited by: Hollinger, J. P., Naval Research Laboratory, Washington, D.C., 1991.

Ridout, A., Ivanova, N., Tonboe, R. T., Rinne, E.: Algorithm Theoretical Basis Document version 1.1 (ATBDv1), 3 October, Doc Ref: SICCI-ATBDv1-04-13, European Space Agency, http://esa-seaice-cci.org (last access: February 2015), 2013.

Röhrs, J. and Kaleschke, L.: An algorithm to detect sea ice leads by using AMSR-E passive microwave imagery, The Cryosphere, 6, 343–352, doi:10.5194/tc-6-343-2012, 2012.

TCD
9, 1269–1313, 2015

Rösel, A., Kaleschke, L., and Birnbaum, G.: Melt ponds on Arctic sea ice determined from MODIS satellite data using an artificial neural network, The Cryosphere, 6, 431–446, doi:10.5194/tc-6-431-2012, 2012a.
Rösel, A., Kaleschke, L., and Kern, S.: Influence of melt ponds on microwave sensor's sea ice concentration retrieval algorithms, Proceedings of Geoscience and Remote Sensing Symposium (IGARSS), 2012 IEEE International, 23–27 July 2012, Munich, 2012b.
Scott, K. A., Buehner, M., and Carrieres, T.: An assessment of sea-ice thickness along the Labrador coast from AMSR-E and MODIS data for operational data assimilation, IEEE T. Geosci. Remote, 52, 2726–2737, 2014.
Shokr, M., Lambe, A., and Agnew, T.: A new algorithm (ECICE) to estimate ice concentration from remote sensing observations: an application to 85-GHz passive microwave data, IEEE T. Geosci. Remote, 46, 4104–4121, 2008.
Smith, D. M.: Extraction of winter total sea-ice concentration in the Greenland and Barents Seas from SSM/I data, Int. J. Remote Sens., 17, 2625–2646, 1996.
Svendsen, E., Kloster, K., Farrelly, B., Johannessen, O. M., Johannessen, J. A., Campbell, W. J., Gloersen, P., Cavalieri, D., and Matzler, C.: Norwegian Remote Sensing Experiment, evaluation of the Nimbus 7 scanning multichannel microwave radiometer for sea ice research, J. Geophys. Res., 88, 2781–2791, 1983.
Swift, C., Fedor, L., and Ramseier, R.: An algorithm to measure sea ice concentration with microwave radiometers, J. Geophys. Res., 90, 1087–1099, 1985.
Tonboe, R. T.: The simulated sea ice thermal microwave emission at window and sounding frequencies, Tellus A, 62, 333–344, 2010.
Tonboe, R. T. and Andersen, S.: Modelled radiometer algorithm ice concentration sensitivity to emissivity variations of the Arctic sea ice snow cover, Danish Meteorological Institute Scientific Report 04-03, Danish Meteorological Institute, Copenhagen, Denmark, 2004.
Tonboe, R. T., Dybkjær, G., and Høyer, J. L.: Simulations of the snow covered sea ice surface temperature and microwave effective temperature, Tellus A, 63, 1028–1037, 2011.
Tschudi, M. A., Maslanik, J. A., and Perovich, D. K.: Derivation of melt pond coverage on arctic sea ice using MODIS observation, Remote Sens. Environ., 112, 2605–2614, 2008.
Wentz, F. J.: A well-calibrated ocean algorithm for SSM/I, J. Geophys. Res., 102, 8703–8718, 1997.
Wentz, F. J., Ricciardulli, L., Hilburn, K. A., and Mears, C. A.: How much more rain will global warming bring?, Science, 317, 233–235, 2007.

TCD
9, 1269–1313, 2015

Table 1. The selection of thirteen sea ice algorithms shown in this study.

Algorithm	Acronym	Reference	Channels
Bootstrap P	BP	Comiso (1986)	37V, 37H ***P***
CalVal	CV	Ramseier (1991)	19, 37V ***F***
Bristol	BR	Smith (1996)	19, 37V, 37H ***PF***
NASA Team	NT	Cavalieri et al. (1984)	19V, 19H, 37V ***PF***
ASI	ASI	Kaleschke et al. (2001)	85V, 85H ***P***
Near 90 GHz linear	N90	Ridout et al. (2013)	85V, 85H ***P***
ESMR	ESMR	Parkinson et al. (2004)	19H
6H	6H	Pedersen (1994)	6H
ECICE	ECICE	Shokr et al. (2008)	19V and 19H or 37V and 37H ***P***
NASA Team 2	NT2	Markus and Cavalieri (2000)	19V, 19H, 37, 85V, 85H ***PF***
NT+CV	NT+CV	Ridout et al. (2013)	19V, 19H, 37V ***PF***
CV+N90	CV+N90	Ridout et al. (2013)	19, 37, 85V, 85H ***PF***
OSISAF	OSISAF	Eastwood (Ed.) (2012)	19, 37V, 37H ***PF***

P indicates that the algorithm is based on the polarisation difference or ratio at a single frequency;
F indicates that the algorithm uses two different frequencies at the same polarisation (i.e. a spectral gradient). The names of the high-frequency algorithms (and the algorithms partially using high frequencies) are shown in bold, while the rest are low-frequency algorithms.

TCD
9, 1269–1313, 2015

Table A1. The RRDP Tie-points: brightness temperatures in K.

	AMSR-E			SSM/I			SMMR		
	OW	FYI	MYI	OW	FYI	MYI	OW	FYI	MYI
Northern Hemisphere									
6V	161.35	251.99	246.04				153.79	251.99	246.04
6H	82.13	232.08	221.19				86.49	232.08	221.19
10V	167.34	251.34	239.61				161.81	251.34	239.61
10H	88.26	234.01	216.31				95.59	234.01	216.31
18V	183.72	252.15	226.26	185.04	252.79	223.64	176.99	252.15	226.26
18H	108.46	237.54	207.78	117.16	238.20	206.46	111.45	237.54	207.78
22V	196.41	250.87	216.67	200.19	250.46	216.72	185.93	250.87	216.67
22H	128.23	236.72	199.60				135.98	236.72	199.60
37V	209.81	247.13	196.91	208.72	244.68	190.14	207.48	247.13	196.91
37H	145.29	235.01	184.94	149.39	233.25	179.68	147.67	235.01	184.94
85V	243.20	232.01	187.60	243.67	225.54	180.55			
85H	196.94	222.39	178.90	205.73	217.21	173.59			
Southern Hemisphere									
6V	159.69	257.04	254.18				148.60	257.04	254.18
6H	80.15	236.52	225.37				83.47	236.52	225.37
10V	166.31	257.23	251.65				159.12	257.23	251.65
10H	86.62	238.50	221.47				93.80	238.50	221.47
18V	185.34	258.58	246.10	185.02	259.92	246.27	175.39	258.58	246.10
18H	110.83	242.80	217.65	118.00	244.57	221.95	110.67	242.80	217.65
22V	201.53	257.56	240.65	198.66	257.85	242.01	186.10	257.56	240.65
22H	137.19	242.61	213.79				129.63	242.61	213.79
37V	212.57	253.84	226.51	209.59	254.39	226.46	207.57	253.84	226.51
37H	149.07	239.96	204.66	152.24	241.63	207.57	149.60	239.96	204.66
85V	247.59	242.81	210.22	242.41	244.84	211.98			
85H	207.20	232.40	197.78	206.12	235.76	200.88			

TCD
9, 1269–1313, 2015

Table B1. Trends in y component of ice tie-points in Bristol scheme (BR ice), average for BR ice, and trends in open water tie-points (Tb19V ow and Tb37V ow) in $K yr^{-1}$ for the overlap periods.

Parameter	BR ice	BR ice avrg	Tb19V ow	Tb37V ow
Northern Hemisphere				
May 1992 to May 1997 of f10 and f11				
f10	0.033	103.2	−0.01	−0.04
f11	−0.061	103.0	0.02	−0.04
May 1995 to May 1999 of f11 and f13				
f11	−0.086	103.5	0.00	−0.04
f13	−0.114	103.7	0.05	−0.05
May 2000 to May 2006 of f13, f14 and f15				
f13	−0.009	104.1	0.02	−0.08
f14	−0.047	104.0	0.00	0.01
f15	0.024	104.0	−0.04	−0.01
May 1997 to May 2008 of f13 and f14				
f13	−0.027	104.0	0.02	−0.05
f14	−0.027	103.9	0.00	0.01
Southern Hemisphere				
May 1992 to May 1997 of f10 and f11				
f10	−0.068	103.1	0.01	0.00
f11	0.072	103.0	0.06	−0.02
May 1995 to May 1999 of f11 and f13				
f11	−0.223	102.6	0.01	−0.02
f13	−0.197	102.6	−0.04	−0.01
May 2000 to May 2006 of f13, f14 and f15				
f13	−0.034	103.3	−0.02	−0.03
f14	−0.077	103.3	0.02	−0.01
f15	−0.042	103.3	−0.04	0.00
May 1997 to May 2008 of f13 and f14				
f13	0.049	103.1	−0.02	−0.01
f14	0.020	103.1	0.02	−0.01

TCD
9, 1269–1313, 2015

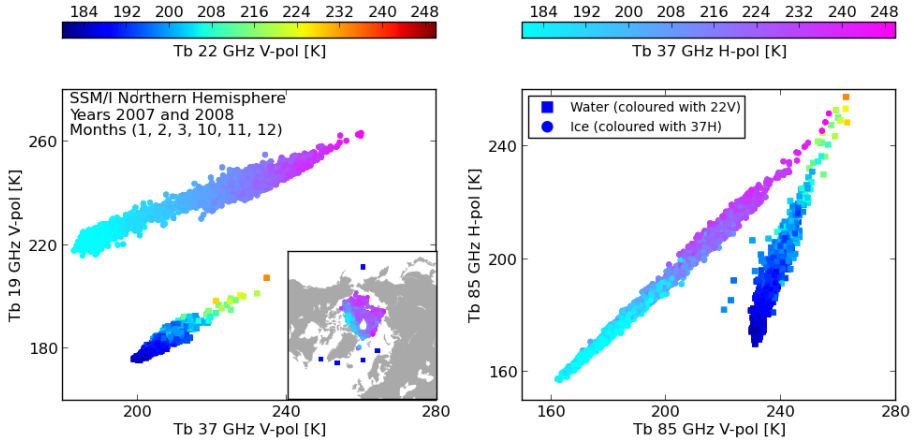

Figure 1. Coverage graphs for the SSM/I subset of Northern Hemisphere RRDP in winters 2007 and 2008. Both the Tb and spatial coverage are displayed. In all panels, square symbols are used for the Open Water locations, and circles for Closed Ice.

TCD
9, 1269–1313, 2015

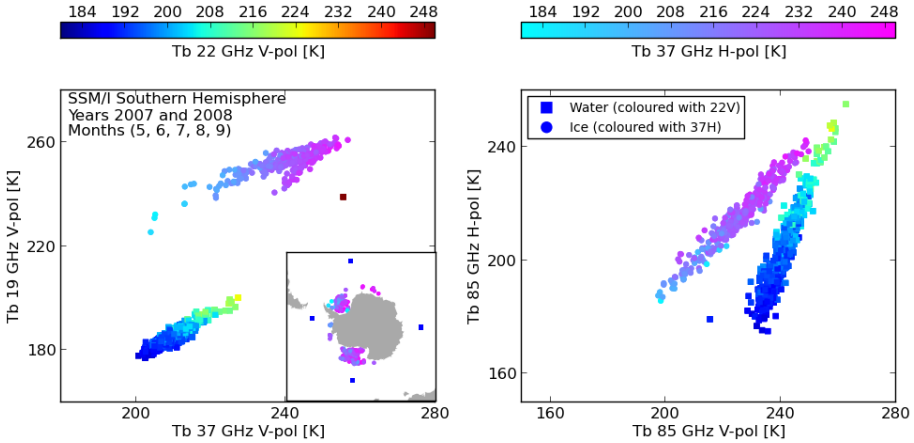

Figure 2. Same as Fig. 1, but in the Southern Hemisphere.

TCD
9, 1269–1313, 2015

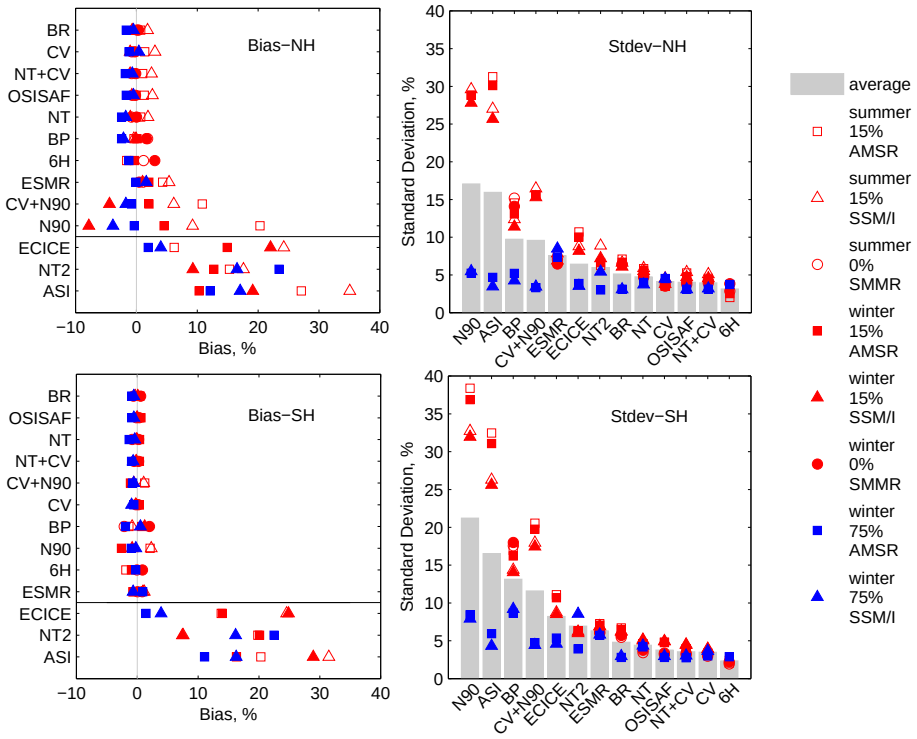

Figure 3. SIC bias and SD (in %) for the Northern (upper panels) and Southern (bottom panels) Hemispheres retrieved without open water filter applied. Grey bars: average values (15 and 75 %, weighted for each instrument depending on length of potential dataset). The algorithms above the black lines on the left panels have RRDP tie-points implemented, while the others (ECICE, NT2, and ASI) are used with their own original tie-points. See Table 1 for the algorithms' acronyms.

TCD
9, 1269–1313, 2015

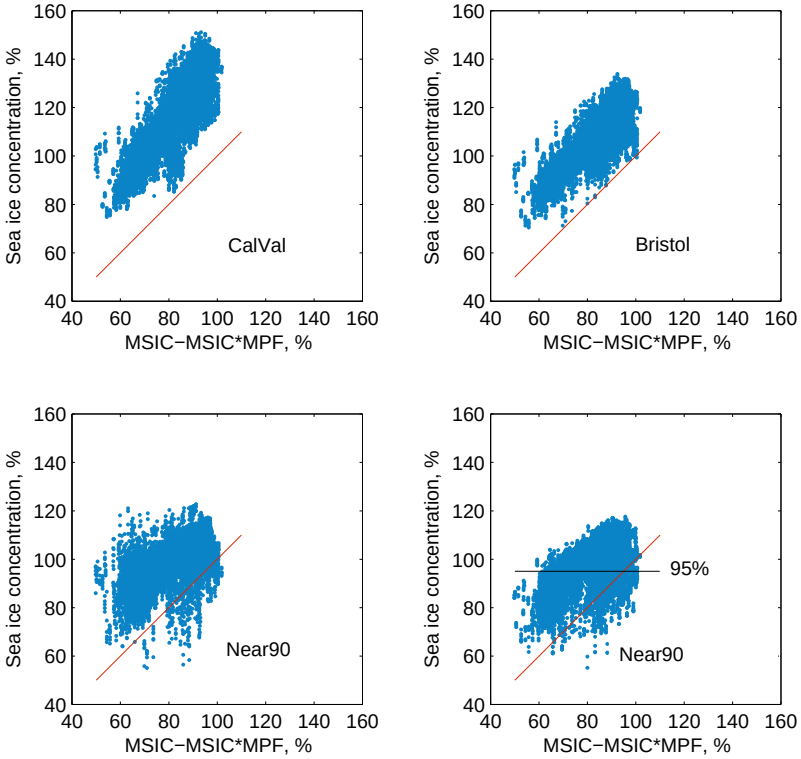

Figure 4. Arctic Ocean AMSR-E SIC from four algorithms in % (y axis) as a function of the net sea ice fraction (MODIS sea ice concentration MSIC minus melt pond fraction MPF) obtained by MODIS for 21 June–31 August 2009. MSIC and MPF are bias-corrected by +3 and −8 %, respectively, relative to Rösel et al. (2012a) following the results of Mäkynen et al. (2014). The red lines show the one-to-one regressions. The black line shows the 95 % SIC for NT (the limit used for the dynamic ice tie-point).

TCD
9, 1269–1313, 2015

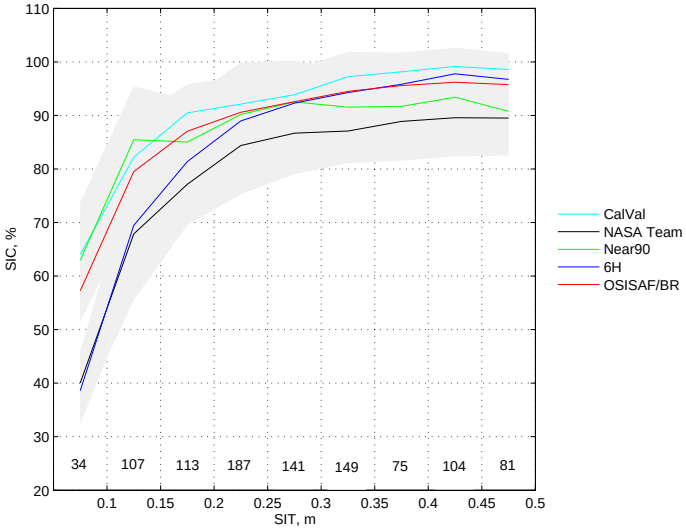

Figure 5. SIC calculated by the implemented algorithms as a function of SMOS ice thickness in areas of the Arctic Ocean, which are known to be 100 % ice during the time period from 1 October to 12 December 2010. Grey shading shows SDs of the algorithms. Number of measurements in each bin is shown above the *x* axis (total number is 991). In this SIC range OSISAF is the same as BR.

TCD
9, 1269–1313, 2015

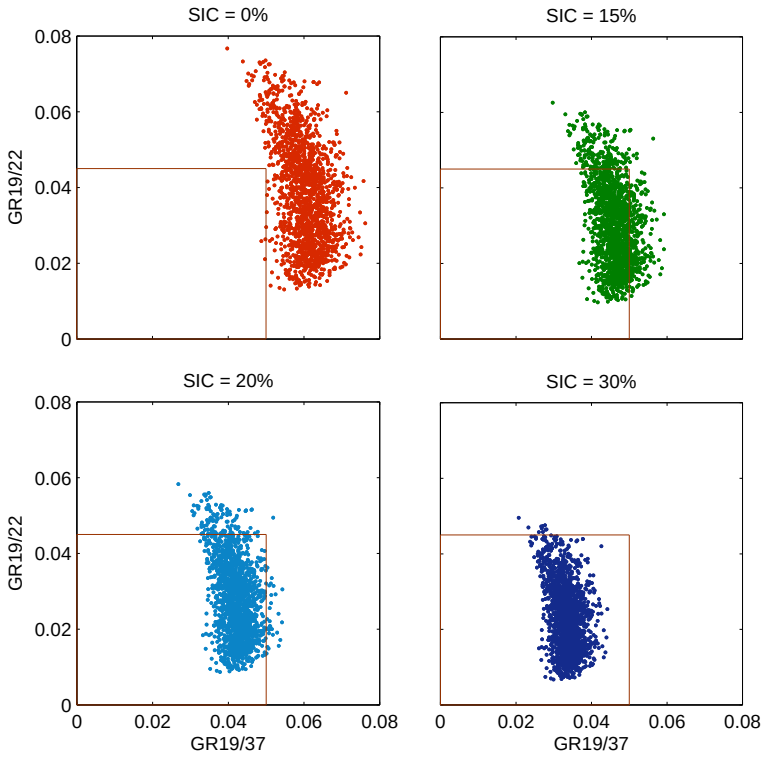

Figure 6. Demonstration of the open water/weather filter performance: gradient ratio (GR) 19/22 is plotted as a function of GR19/37 for SSM/I data in 2008 (full year) for the Northern Hemisphere for SIC of 0, 15, 20 and 30 %. The red square shows the value range outside which the open water/weather filter sets SIC values to 0 % (open water).

TCD
9, 1269–1313, 2015

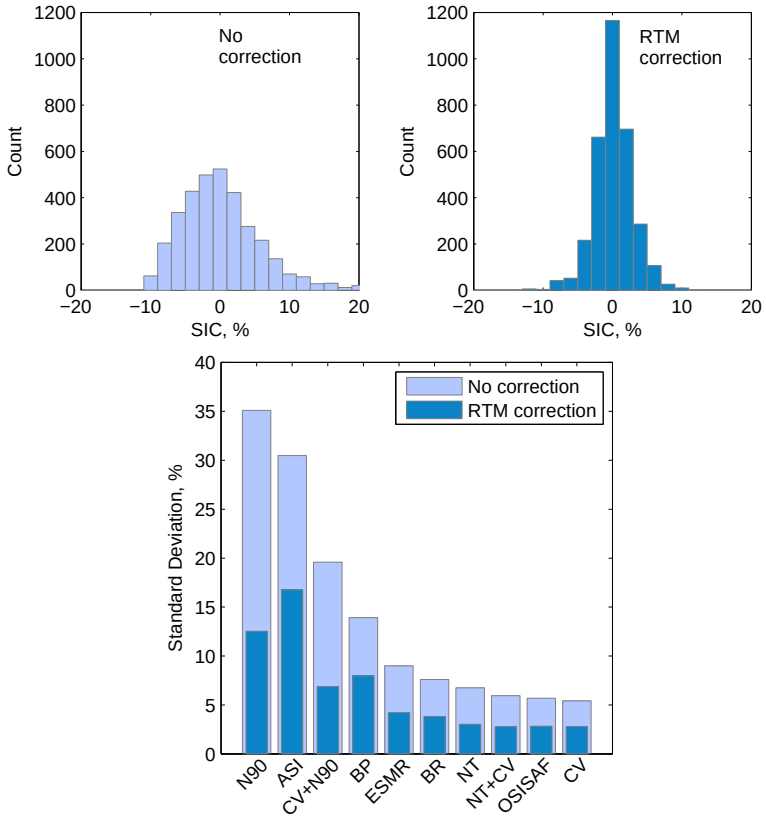

Figure 7. Histograms for the OSISAF algorithm SSM/I SIC over open water (SIC = 0 %) in the Northern Hemisphere in 2008 (full year) without correction (upper left panel) and with RTM correction (upper right panel). The histograms contain 21 bins of 2 % SIC. Bottom panel: decrease in SDs due to the correction of the atmospheric influence on the measured Tb.

TCD
9, 1269–1313, 2015

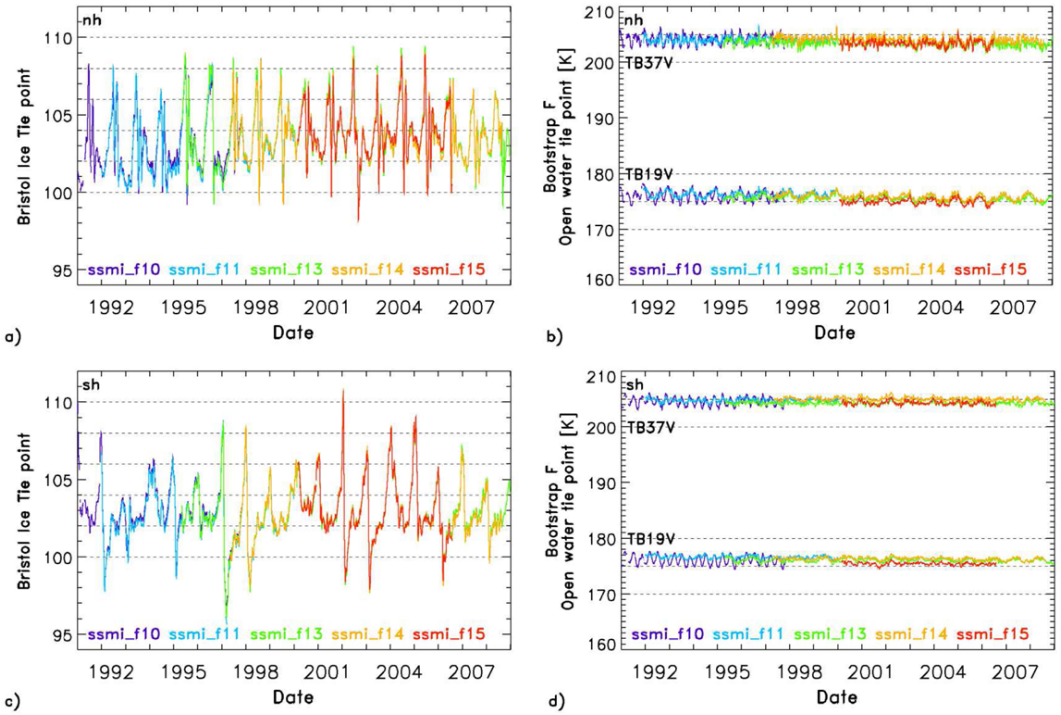

Figure 8. Examples of tie-point time series for BR ice tie-point for the Northern **(a)** and Southern **(c)** Hemispheres and BF open water tie-point (Tb19V and Tb37V) for the Northern **(b)** and Southern **(d)** Hemispheres.

TCD
9, 1269–1313, 2015